PROCEEDINGS OF SCIENCE

The Fitting Procedure for Longitudinal Shower Profiles Observed with the Fluorescence Detector of the Pierre Auger Observatory

José Bellido[a,*] **on behalf of the Pierre Auger Collaboration**[b]

[a] *The University of Adelaide, North Terrace, South Australia, Australia*

[b] *Observatorio Pierre Auger, Av. San Martín Norte 304, 5613 Malargüe, Argentina*

E-mail: spokespersons@auger.org

The Pierre Auger Observatory uses fluorescence telescopes in conjunction with ground level particle detectors to measure high-energy cosmic rays and reconstruct, with greater precision, their arrival direction, their energy and the depth of shower maximum. The depth of shower maximum is important to infer cosmic ray mass composition. The fluorescence detector is capable of directly measuring the longitudinal shower development, which is used to reconstruct the cosmic ray energy and the atmospheric depth of shower maximum. However, given the limited field of view of the fluorescence detector, the shower profile is not always fully contained within the detector observation volume. Therefore, considerations need to be taken in order to reconstruct some events. In this contribution we will describe the method that the Pierre Auger Collaboration uses to reconstruct the longitudinal profiles of showers and present the details of its performance, namely its resolution and systematic uncertainties.

The 38th International Cosmic Ray Conference (ICRC2023)
26 July – 3 August, 2023
Nagoya, Japan

*Speaker

PoS(ICRC2023)211

1. Introduction

At lower energies Auger showers land close to a fluorescence detector and only a small fraction of their profile ends up within the field of view. In these cases the estimation of the calorimetric energy (the integral of the energy deposit) requires a significant extrapolation of the fit function beyond the range of the measurements. HEAT is a set of three fluorescence telescopes installed next to the Coihueco fluorescence detectors (FD) site. HEAT telescopes have a field of view (FoV) ranging from $30°$ to $60°$ in elevation, while the Coihueco FoV ranges from $1.6°$ up to $30°$. The HeCo system (HEAT and Coihueco telescope) helps to extend the FoV, but for lower energies the HeCo FoV is still not large enough. Therefore, “long” track lengths are not common at low energies, and we are forced to introduce constrains to fit shower development profiles in order to reduce the X_{max} and energy reconstruction biases.

2. The Gaisser-Hillas function

The Gaisser-Hillas (GH) function is used to fit the shower development profile. Originally, the GH function was expressed in terms of (X_0, λ) [1]:

$$f_{\text{GH}}^{\lambda,X_0}(X) = (dE/dX)_{\text{max}} \left(\frac{X - X_0}{X_{\text{max}} - X_0} \right)^{\frac{X_{\text{max}} - X_0}{\lambda}} \exp\left(\frac{X_{\text{max}} - X}{\lambda} \right) , \tag{1}$$

which has four parameters: the maximum energy deposit, $(dE/dX)_{\text{max}}$, the depth at which this maximum is reached, X_{max}, and shape parameters X_0 and λ. A mathematically equivalent representation of the GH function can be written in terms of parameters R and L [2]:

$$f_{\text{GH}}^{R,L}(X) = (dE/dX)_{\text{max}} \left(1 + \frac{R(X - X_{\text{max}})}{L} \right)^{R^{-2}} \exp\left(\frac{-(X - X_{\text{max}})}{RL} \right) , \tag{2}$$

where

$$R = \sqrt{\lambda/|X_0'|}, \quad L = \sqrt{|X_0'|\lambda} \quad \text{and} \quad X_0' = X_0 - X_{\text{max}}. \tag{3}$$

The properties of the coefficients (X_0, λ) and (R, L) are different. Below we explore these differences and will show that it is more convenient to use the $f_{\text{GH}}^{R,L}$ to fit the shower profile, applying constraints to the coefficients (R, L).

2.1 Properties of the coefficients (X_0, λ) and (R, L)

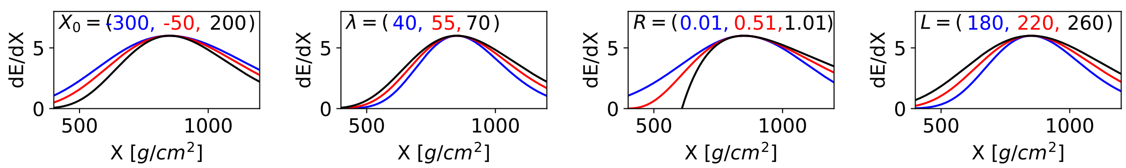

Figure 1: Shape of the GH function when changing only X_0, λ, R and L respectively. The units for dE/dX is [PeV/(g/cm^2)].

Figure 1 shows how the shape of the GH function changes when varying (X_0, λ) or (R, L). The width of the shower profile increases for smaller values of X_0, but also for larger values of λ. This gives rise to a strong correlation between X_0 and λ. Figure 2 shows shower profile fit correlations using the GH functions $f_{\rm GH}^{\lambda,X_0}$ and $f_{\rm GH}^{R,L}$. When performing unconstrained shower profile fits, we only considered profiles longer than 600 g/cm^2 and with $X_{\rm max}$ within the FoV. The observed correlation between R and L is negligible compared to the correlation between X_0 and λ.

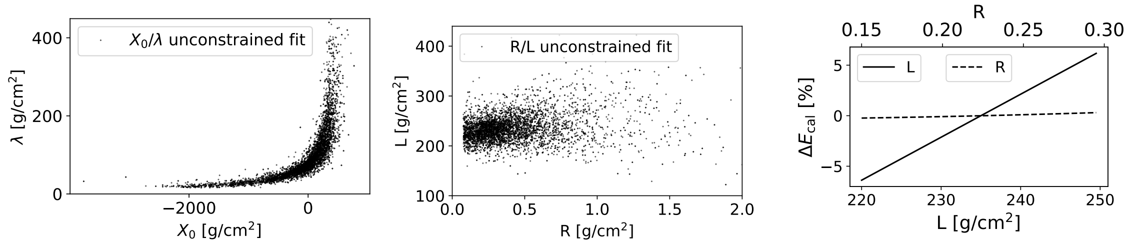

Figure 2: Correlation between reconstructed X_0 and λ (left) and between reconstructed R and L (middle). Change in calorimetric energy as a function of changing L or R (right).

The right panel in Figure 2 shows the variation of the GH function integral (i.e. the calorimetric energy) over reasonable ranges of R and L . $E_{\rm cal}$ is directly proportional to L [2]. The impact of changing R over a reasonable range is negligible, less than 0.3%.

2.2 Correlation of the coefficients (X_0, λ) or (R, L) with Energy and with $X_{\rm max}$

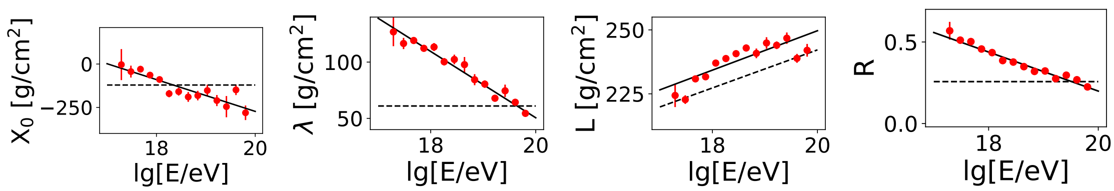

Figure 3: Unconstrained fit results of real data: mean values for X_0, λ, L and R as a function of energy. The solid lines correspond to linear fits. The dashed lines correspond to the central values of the constraints used in a constrained shower profile fit.

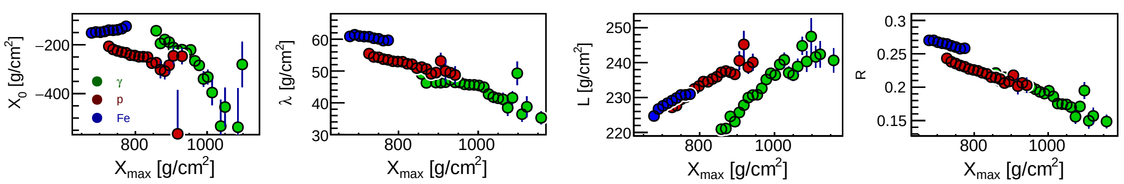

Figure 4: Unconstrained fit results of CONEX shower (Sibyll2.3d, E = 10^{19} eV) profiles for iron (blue), protons (red) and gamma-rays (green). Correlation between reconstructed X_0, λ, L and R with $X_{\rm max}$.

Figures 3 and 4 show the correlation of the Gaisser-Hillas coefficients with energy and $X_{\rm max}$ respectively. There is a physical correlation of the GH coefficients with energy and $X_{\rm max}$. For Figure 4, CONEX simulated showers were used. Physical correlations should be considered when performing constrained shower profile fits. The correlations of X_0 and λ with energy or $X_{\max}$ are complicated to quantify, given the strong correlation between X_0 and λ. On the other hand, the correlations of L are easy to consider and R variations represent negligible changes in the shape of the shower profile.

3. Definition of the constraints in the fit of the shower profile

Constraints on the shape parameters were first implemented in the χ^2 minimization of the Auger longitudinal profile [3] and are currently part of the profile likelihood fit as

$$\mathcal{L} = \mathcal{L}_{\text{GH}}\, G(p_1; \langle p_1 \rangle, \sigma_{p_1})\, G(p_2; \langle p_2 \rangle, \sigma_{p_2}), \tag{4}$$

where $\mathcal{L}_{\text{GH}}$ is the likelihood for the fit of the energy deposit (Poissonian distribution in the number of photoelectrons) and $G(p_i; \langle p_i \rangle, \sigma_{p_i})$ are Gaussian distributions for the shape parameters with variance $\sigma^2_{p_i}$ and centred at the mean values $\langle p_i \rangle$. The shape parameters (p_1, p_2) can be (X_0, λ) or (L, R) depending on whether we use $f_{\text{GH}}^{\lambda,X_0}$ or $f_{\text{GH}}^{R,L}$ to fit the shower profile.

The methods to derive $\langle p_i \rangle$ and σ_{p_i} are of crucial importance to avoid biases in the shape of the profile. These can introduce biases in the calorimetric energy E_{cal} and $X_{\max}$. For that reason, the analysis attempts to derive $\langle p_i \rangle$ from a study of real data. The values of σ_{p_i} are chosen so that they are large enough to avoid biases, but not too large in order to have an efficient constraint for showers with short track lengths.

3.1 Constraints to the $f_{\text{GH}}^{\lambda,X_0}$ function in the shower profile fit

Initially the $f_{\text{GH}}^{\lambda,X_0}$ function was used to fit the shower profiles. For the reconstruction of the data up to ICRC 2015 only X_0 and λ were constrained (this includes data for the energy scale update presented at ICRC 2013 [4] and for the $X_{\max}$ publication [5]), but for the data presented at the ICRC 2017, a constraint to the width of the shower profile was also included in the fit [6].

3.1.1 Constraints to X_0 and λ

The constraints for X_0 and λ were estimated from data. There, X_0 and λ were determined iteratively, where either X_0 or λ were fixed to the value obtained in the previous iteration. The problem with this procedure is that the values obtained depend very much on the starting parameter. Once e.g. an initial X_0 is picked, one recovers immediately the corresponding λ parameter and vice versa (as suggested by left panel in Figure 2). Therefore, one of the central values is arbitrary (either X_0 or λ), which depends on the arbitrary choice of the starting parameter. The average values and variances for the mean and standard deviation of the X_0 and λ distributions are:

$$\langle X_0 \rangle = -120.5 \text{ g/cm}^2 \qquad \sigma_{X_0} = 171.7 \text{ g/cm}^2 \tag{5}$$

$$\langle \lambda \rangle = 60.93 \text{ g/cm}^2 \qquad \sigma_\lambda = 12.93 \text{ g/cm}^2 \tag{6}$$

They are used in the likelihood of the profile fit defined according to Eq. 4, using two independent Gaussian distributions,

$$\mathcal{L} = \mathcal{L}_{\text{GH}}\, G(X_0; \langle X_0 \rangle, \sigma_{X_0})\, G(\lambda; \langle \lambda \rangle, \sigma_\lambda) \tag{7}$$

3.1.2 Adding a constraint to the shower profile width

After the update of the energy scale presented at ICRC 2013, it was realized that the energy estimation for low energy events was affected by a rather large negative bias. In 2015 evidence was found in the data for "non-physical" values of the ratio of the calorimetric energy (the integral of the shower profile) and $(dE/dX)_{\mathrm{max}}$ (the amplitude of the shower profile) for lower energy showers (Fig. 5, left). This ratio was called k, and is approximately *universal* among different primaries and hadronic interaction models as shown in Figure 5 (right). The value of k is a measure of the width of the shower profile in units of g/cm^2,

$$k = \frac{E_{\mathrm{cal}}}{(dE/dX)_{\mathrm{max}}}. \tag{8}$$

From simulations, the mean value of the expected k distribution changes from around 560 to 635 g/cm^2 over the energy range from 10^{17} to 10^{20} eV (black solid line in Figure 5). The plot on the left in Figure 5 corresponds to the reconstructed average k values using real events (HeCo and FD events). The small k values reconstructed at lower energies are biased. The most straightforward solution to remove such a bias was to add a further Gaussian constraint on k in the fit of the shower profile,

$$\mathcal{L} = \mathcal{L}_{\mathrm{GH}}\, G(X_0; \langle X_0\rangle, \sigma_{X_0})\, G(\lambda; \langle\lambda\rangle, \sigma_\lambda)\, G\left(k; \langle k(E_{\mathrm{cal}})\rangle, \sigma_k\right) \tag{9}$$

where the mean value of k is a function of the calorimetric energy.

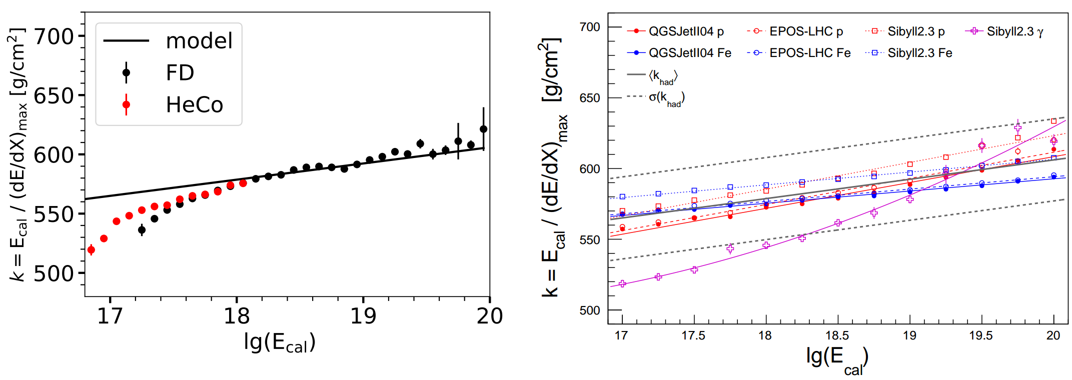

Figure 5: (left) Reconstructed mean k values in real data. The solid line correspond to the average k over all compositions and models (see plot on the right). (right) Predicted mean of the k distribution as a function of energy, for different compositions and hadronic models. The overall average $\langle k_{\mathrm{had}}\rangle$ and the corresponding range for $\sigma(k_{\mathrm{had}})$ are indicated with black solid and dashed lines respectively.

The optimal values of $\langle k\rangle$ and σ_k had to be derived from simulations . The parameterization of $\langle k\rangle$ was obtained from the average of the QGSJetII–04, EPOS–LHC, and Sibyll2.3 predictions with a mixed proton and iron composition shown in Figure 5 (right). The value of σ_k was set in order to account for the different models, mass compositions and the shower-to-shower fluctuations. The parameterizations are [6]:

$$\langle k(E_{\mathrm{cal}})\rangle = \left(332.6 + 13.67\ \log_{10} E_{\mathrm{cal}}\right)\ \mathrm{g/cm^2} \qquad \sigma_k = 29\ \mathrm{g/cm^2} \tag{10}$$

3.2 Constraints to the $f_{\mathrm{GH}}^{R,L}$ function in the shower profile fit

The $f_{\mathrm{GH}}^{R,L}$ function was used in the shower profile fit for the ICRC 2019 data production and for this conference it was improved by refining the probability density function for the L parameter.

3.2.1 Constraints that assume a Gaussian distribution for the L and R parameters

The shower profile fit using the $f_{\mathrm{GH}}^{R,L}$ function was introduced after the publication, in 2019, of the paper on the measurement of the average shape of longitudinal profiles [7]. It was consequently used for the ICRC 2019 and ICRC 2021 data production and for the papers on the energy spectrum obtained with the 1500 m [8, 9] and 750 m [10] arrays.

The fit with the $f_{\mathrm{GH}}^{R,L}$ function has several advantages. The parameter L is to a very good approximation equivalent to k since $L \simeq k/\sqrt{2\pi}$, and therefore a fit very similar to that defined by Eq. 9 can be performed using only two constraints:

$$\mathcal{L} = \mathcal{L}_{\mathrm{GH}}\, G(L; \langle L\rangle, \sigma_L)\, G(R; \langle R\rangle, \sigma_R) \tag{11}$$

Moreover, the average values of the shape parameters can be fixed using the measurements presented in [7], therefore improving the old approach where $\langle k\rangle$ was fixed using MC simulations.

The σ of the constraints were defined following the same logic used for σ_k. The one for L has been derived from that used for k ($\sigma_L = \sigma_k/\sqrt{2\pi}$), while for R we have done a dedicated study using MC simulations. The final parameterizations are:

$$\langle L\rangle = \left[227.3 + 7.44\ \left(\log_{10} E_{\mathrm{cal}} - 18\right)\right]\ \mathrm{g/cm^2} \qquad \sigma_L = 11.5\ \mathrm{g/cm^2} \tag{12}$$

$$\langle R\rangle = 0.257 \qquad \sigma_R = 0.055 \tag{13}$$

The systematic uncertainties in the measurements of $\langle L\rangle$ and $\langle R\rangle$ are 7.3 $\mathrm{g/cm^2}$ and 0.040 respectively, well below the σ of the constraints.

3.2.2 Constraints that assume an exponentially modified Gaussian distribution for the L parameter

From shower simulations we noticed that the R distributions are rather symmetric and the width of the constraint looks large enough to encompass the shower-to-shower fluctuations. However, the situation for the L parameter is more complicated: while the distribution for iron showers is rather narrow and symmetric, the one for protons has a long tail toward large values of L and the constraint is clearly not large enough to encompass all the values of L. We noticed that a small bias in $X_{\max}$ was introduced for deep showers when the asymmetric distribution of L was not taken into account.

The L distributions for proton showers for different ranges of $X_{\max}$ are well described by an exponentially modified Gaussian, i.e. the convolution of the normal and exponential probability density functions,

$$G_{\exp} = e^{-x/\tau_L} \otimes \frac{1}{\sigma_L\sqrt{2\pi}} e^{-(x-\mu)^2/2\sigma_L^2} = \frac{1}{2\tau_L} \exp\left(\frac{1}{\tau_L}\left(-x+\mu+\frac{\sigma_L^2}{2\tau_L}\right)\right) \mathrm{erfc}\left(\frac{-x+\mu+\sigma_L^2/\tau_L}{\sqrt{2}\sigma_L}\right) \tag{14}$$

where τ_L characterizes the exponential decay and erfc is the complementary error function.

For proton showers the value for τ_L/σ_L increases linearly with $X_{\max}$, regardless of the shower energy. For shallow $X_{\max}$ ($X_{\max}$ = 700 g/cm^2) $\tau_L/\sigma_L = 1$, and for deep showers ($X_{\max}$ = 1000 g/cm^2) $\tau_L/\sigma_L = 3$. For iron showers all the L distributions are well described by a normal p.d.f. with $\tau_L/\sigma_L \approx 0.6$.

The study of the L distributions has led to a new definition of the likelihood for the fit with the $f_{\mathrm{GH}}^{R,L}$ function. In this new version, the R constraint is the same as the one defined in Section 3.2.1 and the one for L is given by an exponentially modified Gaussian p.d.f.:

$$\mathcal{L} = \mathcal{L}_{\mathrm{GH}}\, G_{\exp}(L; \langle L_M \rangle, \sigma_L, \tau_L/\sigma_L)\; G(R; \langle R \rangle, \sigma_R) \tag{15}$$

$G_{\exp}$ is characterized by three parameters: L_M is the *Mode* (value of L for which the p.d.f. has its maximum) and its mean value is parametrized as a function of E_{cal} with Equation 12 using the measurements of the average shape of the longitudinal profiles [7] (justified by the fact that in the bulk of the data there are not so many deep showers), $\sigma_L = 11.5$ g/cm^2 (the same of the Gaussian constraint, see Equation 12) and τ_L/σ_L is conservatively fixed to the maximum value observed in simulated events, $\tau_L/\sigma_L = 3$ (corresponding to $\tau_L = 34.5$ g/cm^2). The resulting p.d.f. for the L constraint, in comparison to the Gaussian constraint, is now large enough to encompass the shower-to-shower fluctuations even for the very deep showers.

4. Performance of the constrained fit of the shower profile

Figure 6 show the biases in reconstructed $X_{\max}$ and energy as a function of $X_{\max}$ for three different types of fit constraints. Panels on the left show the biases calculated using simulated events at energies between $10^{17.8}$ eV and $10^{18.5}$ eV. Panels on the right show relative reconstruction differences in real events for energies between $10^{18.5}$ eV and $10^{19.0}$ eV. The biases for $f_{\mathrm{GH}}^{R,L}G$ and $f_{\mathrm{GH}}^{R,L}G_{\exp}$ fits are rather small (left plots), with a slightly better performance for the $f_{\mathrm{GH}}^{R,L}G_{\exp}$ fit. In contrast, the $f_{\mathrm{GH}}^{\lambda,X_0}$ fit shows a rather large positive bias in E_{cal} for deep showers. This bias looks correlated with the positive bias also observed for $X_{\max}$. This is not surprising because, $f_{\mathrm{GH}}^{\lambda,X_0}$ fit tends to overestimate the profile width L when the showers are deep. Larger profile widths clearly correspond to larger values of E_{cal}, and when the profile size is increased the fit tends to introduce a positive bias in $X_{\max}$. The relative differences observed using real events take as reference the $f_{\mathrm{GH}}^{R,L}G$ fit, and they are for intermediate energies, between $10^{18.5}$ eV and 10^{19} eV.

The relative difference between $f_{\mathrm{GH}}^{R,L}G_{\exp}$ and $f_{\mathrm{GH}}^{R,L}G$ fits show a moderate $X_{\max}$ dependence. In the most extreme case for $X_{\max} \approx 1000$ g/cm^2, the difference maximize at about 6 g/cm^2 for $X_{\max}$ and 3% for energy. The $f_{\mathrm{GH}}^{\lambda,X_0}$ fit gives shifts consistent with those of the $f_{\mathrm{GH}}^{R,L}G_{\exp}$ fit, within 2 g/cm^2 and 1%, with the exception of the few events with $X_{\max} \approx 1000$ g/cm^2.

For higher energies, above 10^{19} eV, the shifts are very small which means that the performance of the three fits are very similar. This is to some extent expected, as at the highest energies the statistical fluctuations of the measured dE/dX are small and the profiles are in general well contained in the field of view of the telescopes.

5. Conclusion

In some cases the estimation of the calorimetric energy requires a significant extrapolation of the fit function beyond the range of the measurements. The constraints in the parameters that

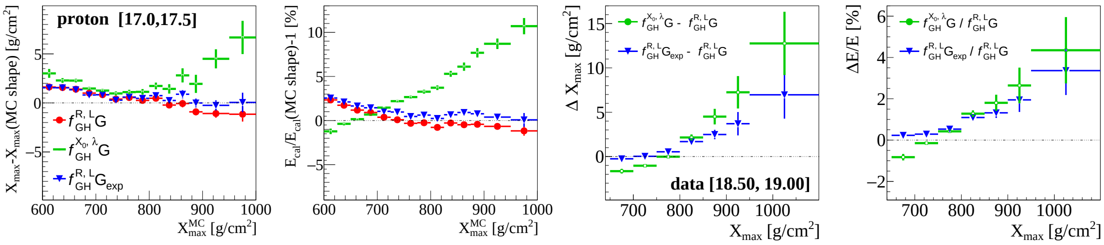

Figure 6: (left) X_{max} and E_{cal} biases of the profile fit for the HECO events simulated with Sibyll 2.3d (simulations include a realistic energy spectrum and real atmosphere characteristics). The events were selected using appropriate FoV cuts. (right) X_{max} and energy relative difference observed with real data for the $f_{\mathrm{GH}}^{R,L}G_{\mathrm{exp}}$ and the $f_{\mathrm{GH}}^{\lambda,X_0}$ fits taking as a reference the $f_{\mathrm{GH}}^{R,L}G$ fit. Notice that plots on the left and on the right correspond to different energy ranges.

characterize the shape of the shower profile allow us to take control of the extrapolation. This is particularly important at low energies where the showers are characterized by relatively short track lengths. We have carefully examined the impact on the energy reconstruction of various types of constrained fit. The improvement in the energy resolution and the better control of systematic uncertainties is remarkable when the shower width "L" is constrained in the fit of $f_{\mathrm{GH}}^{R,L}$ to the measured profiles.

References

[1] T.K. Gaisser and A.M. Hillas. "Reliability of the method of constant intensity cuts for reconstructing the average development of vertical showers". In: *proceedings of the 15th International Cosmic Ray Conference (ICRC 1977), August 13–26, Plovdiv, Bulgaria*. 1977.

[2] S. Andringa, R. Conceição, and M. Pimenta. "Mass composition and cross-section from the shape of cosmic ray shower longitudinal profiles". In: *Astroparticle Physics* 34.6 (2011), pp. 360–367. ISSN: 0927-6505. DOI: https://doi.org/10.1016/j.astropartphys.2010.10.002. URL: https://www.sciencedirect.com/science/article/pii/S0927650510001830.

[3] M. Unger et al. "Reconstruction of Longitudinal Profiles of Ultra-High Energy Cosmic Ray Showers from Fluorescence and Cherenkov Light Measurements". In: *Nucl. Instrum. Meth. A* 588 (2008), pp. 433–441. DOI: 10.1016/j.nima.2008.01.100. arXiv: 0801.4309 [astro-ph].

[4] V. Verzi. "The Energy Scale of the Pierre Auger Observatory". In: *Proceedings of the 33rd International Cosmic Ray Conference, Rio de Janeiro, Brazil* (2013). arXiv: 1307.5059.

[5] A. Aab et al. "Depth of maximum of air-shower profiles at the Pierre Auger Observatory. I. Measurements at energies above $10^{17.8}$ eV". In: *Phys. Rev. D* 90 (12 Dec. 2014), p. 122005. DOI: 10.1103/PhysRevD.90.122005. URL: https://link.aps.org/doi/10.1103/PhysRevD.90.122005.

[6] Francesco Fenu. "The cosmic ray energy spectrum measured using the Pierre Auger Observatory". In: *Proceedings of 35th International Cosmic Ray Conference — PoS(ICRC2017)*. Vol. 301. 2017, p. 486. DOI: 10.22323/1.301.0486.

[7] Alexander Aab et al. "Measurement of the average shape of longitudinal profiles of cosmic-ray air showers at the Pierre Auger Observatory". In: *JCAP* 03 (2019), p. 018. DOI: 10.1088/1475-7516/2019/03/018. arXiv: 1811.04660 [astro-ph.HE].

[8] Alexander Aab et al. "Features of the Energy Spectrum of Cosmic Rays above $2.5{\times}10^{18}$ eV Using the Pierre Auger Observatory". In: *Phys. Rev. Lett.* 125.12 (2020), p. 121106. DOI: 10.1103/PhysRevLett.125.121106. arXiv: 2008.06488 [astro-ph.HE].

[9] Alexander Aab et al. "Measurement of the cosmic-ray energy spectrum above $2.5{\times}10^{18}$ eV using the Pierre Auger Observatory". In: *Phys. Rev. D* 102.6 (2020), p. 062005. DOI: 10.1103/PhysRevD.102.062005. arXiv: 2008.06486 [astro-ph.HE].

[10] P. Abreu et al. "The energy spectrum of cosmic rays beyond the turn-down around 10^{17} eV as measured with the surface detector of the Pierre Auger Observatory". In: *Eur. Phys. J. C* 81 (2021), p. 966. DOI: 10.1140/epjc/s10052-021-09700-w. arXiv: 2109.13400 [astro-ph.HE].

The Pierre Auger Collaboration

A. Abdul Halim[13], P. Abreu[72], M. Aglietta[54,52], I. Allekotte[1], K. Almeida Cheminant[70], A. Almela[7,12], R. Aloisio[45,46], J. Alvarez-Muñiz[79], J. Ammerman Yebra[79], G.A. Anastasi[54,52], L. Anchordoqui[86], B. Andrada[7], S. Andringa[72], C. Aramo[50], P.R. Araújo Ferreira[42], E. Arnone[63,52], J. C. Arteaga Velázquez[67], H. Asorey[7], P. Assis[72], G. Avila[11], E. Avocone[57,46], A.M. Badescu[75], A. Bakalova[32], A. Balaceanu[73], F. Barbato[45,46], A. Bartz Mocellin[85], J.A. Bellido[13,69], C. Berat[36], M.E. Bertaina[63,52], G. Bhatta[70], M. Bianciotto[63,52], P.L. Biermann[h], V. Binet[5], K. Bismark[39,7], T. Bister[80,81], J. Biteau[37], J. Blazek[32], C. Bleve[36], J. Blümer[41], M. Boháčová[32], D. Boncioli[57,46], C. Bonifazi[8,26], L. Bonneau Arbeletche[21], N. Borodai[70], J. Brack[j], P.G. Brichetto Orchera[7], F.L. Briechle[42], A. Bueno[78], S. Buitink[15], M. Buscemi[47,61], M. Büsken[39,7], A. Bwembya[80,81], K.S. Caballero-Mora[66], S. Cabana-Freire[79], L. Caccianiga[59,49], I. Caracas[38], R. Caruso[58,47], A. Castellina[54,52], F. Catalani[18], G. Cataldi[48], L. Cazon[79], M. Cerda[10], A. Cermenati[45,46], J.A. Chinellato[21], J. Chudoba[32], L. Chytka[33], R.W. Clay[13], A.C. Cobos Cerutti[6], R. Colalillo[60,50], A. Coleman[90], M.R. Coluccia[48], R. Conceição[72], A. Condorelli[37], G. Consolati[49,55], M. Conte[56,48], F. Convenga[41], D. Correia dos Santos[28], P.J. Costa[72], C.E. Covault[84], M. Cristinziani[44], C.S. Cruz Sanchez[3], S. Dasso[4,2], K. Daumiller[41], B.R. Dawson[13], R.M. de Almeida[28], J. de Jesús[7,41], S.J. de Jong[80,81], J.R.T. de Mello Neto[26,27], I. De Mitri[45,46], J. de Oliveira[17], D. de Oliveira Franco[21], F. de Palma[56,48], V. de Souza[19], E. De Vito[56,48], A. Del Popolo[58,47], O. Deligny[34], N. Denner[32], L. Deval[41,7], A. di Matteo[52], M. Dobre[73], C. Dobrigkeit[21], J.C. D'Olivo[68], L.M. Domingues Mendes[72], J.C. dos Anjos, R.C. dos Anjos[25], J. Ebr[32], F. Ellwanger[41], M. Emam[80,81], R. Engel[39,41], I. Epicoco[56,48], M. Erdmann[42], A. Etchegoyen[7,12], C. Evoli[45,46], H. Falcke[80,82,81], J. Farmer[89], G. Farrar[88], A.C. Fauth[21], N. Fazzini[e], F. Feldbusch[40], F. Fenu[41,d], A. Fernandes[72], B. Fick[87], J.M. Figueira[7], A. Filipčič[77,76], T. Fitoussi[41], B. Flaggs[90], T. Fodran[80], T. Fujii[89,f], A. Fuster[7,12], C. Galea[80], C. Galelli[59,49], B. García[6], C. Gaudu[38], H. Gemmeke[40], F. Gesualdi[7,41], A. Gherghel-Lascu[73], P.L. Ghia[34], U. Giaccari[48], M. Giammarchi[49], J. Glombitza[42,g], F. Gobbi[10], F. Gollan[7], G. Golup[1], M. Gómez Berisso[1], P.F. Gómez Vitale[11], J.P. Gongora[11], J.M. González[1], N. González[7], I. Goos[1], D. Góra[70], A. Gorgi[54,52], M. Gottowik[79], T.D. Grubb[13], F. Guarino[60,50], G.P. Guedes[22], E. Guido[44], S. Hahn[39], P. Hamal[32], M.R. Hampel[7], P. Hansen[3], D. Harari[1], V.M. Harvey[13], A. Haungs[41], T. Hebbeker[42], C. Hojvat[e], J.R. Hörandel[80,81], P. Horvath[33], M. Hrabovský[33], T. Huege[41,15], A. Insolia[58,47], P.G. Isar[74], P. Janecek[32], J.A. Johnsen[85], J. Jurysek[32], A. Kääpä[38], K.H. Kampert[38], B. Keilhauer[41], A. Khakurdikar[80], V.V. Kizakke Covilakam[7,41], H.O. Klages[41], M. Kleifges[40], F. Knapp[39], N. Kunka[40], B.L. Lago[16], N. Langner[42], M.A. Leigui de Oliveira[24], Y Lema-Capeans[79], V. Lenok[39], A. Letessier-Selvon[35], I. Lhenry-Yvon[34], D. Lo Presti[58,47], L. Lopes[72], L. Lu[91], Q. Luce[39], J.P. Lundquist[76], A. Machado Payeras[21], M. Majercakova[32], D. Mandat[32], B.C. Manning[13], P. Mantsch[e], S. Marafico[34], F.M. Mariani[59,49], A.G. Mariazzi[3], I.C. Mariş[14], G. Marsella[61,47], D. Martello[56,48], S. Martinelli[41,7], O. Martínez Bravo[64], M.A. Martins[79], M. Mastrodicasa[57,46], H.J. Mathes[41], J. Matthews[a], G. Matthiae[62,51], E. Mayotte[85,38], S. Mayotte[85], P.O. Mazur[e], G. Medina-Tanco[68], J. Meinert[38], D. Melo[7], A. Menshikov[40], C. Merx[41], S. Michal[33], M.I. Micheletti[5], L. Miramonti[59,49], S. Mollerach[1], F. Montanet[36], L. Morejon[38], C. Morello[54,52], A.L. Müller[32], K. Mulrey[80,81], R. Mussa[52], M. Muzio[88], W.M. Namasaka[38], S. Negi[32], L. Nellen[68], K. Nguyen[87], G. Nicora[9], M. Niculescu-Oglinzanu[73], M. Niechciol[44], D. Nitz[87], D. Nosek[31], V. Novotny[31], L. Nožka[33], A Nucita[56,48], L.A. Núñez[30], C. Oliveira[19], M. Palatka[32], J. Pallotta[9], S. Panja[32], G. Parente[79], T. Paulsen[38], J. Pawlowsky[38], M. Pech[32], J. Pękala[70], R. Pelayo[65], L.A.S. Pereira[23], E.E. Pereira Martins[39,7], J. Perez Armand[20], C. Pérez Bertolli[7,41], L. Perrone[56,48], S. Petrera[45,46], C. Petrucci[57,46], T. Pierog[41], M. Pimenta[72], M. Platino[7], B. Pont[80], M. Pothast[81,80], M. Pourmohammad Shahvar[61,47], P. Privitera[89], M. Prouza[32], A. Puyleart[87], S. Querchfeld[38], J. Rautenberg[38], D. Ravignani[7], M. Reininghaus[39], J. Ridky[32], F. Riehn[79], M. Risse[44], V. Rizi[57,46], W. Rodrigues de Carvalho[80], E. Rodriguez[7,41], J. Rodriguez Rojo[11], M.J. Roncoroni[7], S. Rossoni[43], M. Roth[41], E. Roulet[1], A.C. Rovero[4], P. Ruehl[44], A. Saftoiu[73], M. Saharan[80], F. Salamida[57,46], H. Salazar[64], G. Salina[51], J.D. Sanabria Gomez[30], F. Sánchez[7], E.M. Santos[20], E. Santos[32],

F. Sarazin[85], R. Sarmento[72], R. Sato[11], P. Savina[91], C.M. Schäfer[41], V. Scherini[56,48], H. Schieler[41], M. Schimassek[34], M. Schimp[38], F. Schlüter[41], D. Schmidt[39], O. Scholten[15,i], H. Schoorlemmer[80,81], P. Schovánek[32], F.G. Schröder[90,41], J. Schulte[42], T. Schulz[41], S.J. Sciutto[3], M. Scornavacche[7,41], A. Segreto[53,47], S. Sehgal[38], S.U. Shivashankara[76], G. Sigl[43], G. Silli[7], O. Sima[73,b], F. Simon[40], R. Smau[73], R. Šmída[89], P. Sommers[k], J.F. Soriano[86], R. Squartini[10], M. Stadelmaier[32], D. Stanca[73], S. Stanič[76], J. Stasielak[70], P. Stassi[36], S. Strähnz[39], M. Straub[42], M. Suárez-Durán[14], T. Suomijärvi[37], A.D. Supanitsky[7], Z. Svozilikova[32], Z. Szadkowski[71], A. Tapia[29], C. Taricco[63,52], C. Timmermans[81,80], O. Tkachenko[41], P. Tobiska[32], C.J. Todero Peixoto[18], B. Tomé[72], Z. Torrès[36], A. Travaini[10], P. Travnicek[32], C. Trimarelli[57,46], M. Tueros[3], M. Unger[41], L. Vaclavek[33], M. Vacula[33], J.F. Valdés Galicia[68], L. Valore[60,50], E. Varela[64], A. Vásquez-Ramírez[30], D. Veberič[41], C. Ventura[27], I.D. Vergara Quispe[3], V. Verzi[51], J. Vicha[32], J. Vink[83], J. Vlastimil[32], S. Vorobiov[76], C. Watanabe[26], A.A. Watson[c], A. Weindl[41], L. Wiencke[85], H. Wilczyński[70], D. Wittkowski[38], B. Wundheiler[7], B. Yue[38], A. Yushkov[32], O. Zapparrata[14], E. Zas[79], D. Zavrtanik[76,77], M. Zavrtanik[77,76]

[1] Centro Atómico Bariloche and Instituto Balseiro (CNEA-UNCuyo-CONICET), San Carlos de Bariloche, Argentina
[2] Departamento de Física and Departamento de Ciencias de la Atmósfera y los Océanos, FCEyN, Universidad de Buenos Aires and CONICET, Buenos Aires, Argentina
[3] IFLP, Universidad Nacional de La Plata and CONICET, La Plata, Argentina
[4] Instituto de Astronomía y Física del Espacio (IAFE, CONICET-UBA), Buenos Aires, Argentina
[5] Instituto de Física de Rosario (IFIR) – CONICET/U.N.R. and Facultad de Ciencias Bioquímicas y Farmacéuticas U.N.R., Rosario, Argentina
[6] Instituto de Tecnologías en Detección y Astropartículas (CNEA, CONICET, UNSAM), and Universidad Tecnológica Nacional – Facultad Regional Mendoza (CONICET/CNEA), Mendoza, Argentina
[7] Instituto de Tecnologías en Detección y Astropartículas (CNEA, CONICET, UNSAM), Buenos Aires, Argentina
[8] International Center of Advanced Studies and Instituto de Ciencias Físicas, ECyT-UNSAM and CONICET, Campus Miguelete – San Martín, Buenos Aires, Argentina
[9] Laboratorio Atmósfera – Departamento de Investigaciones en Láseres y sus Aplicaciones – UNIDEF (CITEDEF-CONICET), Argentina
[10] Observatorio Pierre Auger, Malargüe, Argentina
[11] Observatorio Pierre Auger and Comisión Nacional de Energía Atómica, Malargüe, Argentina
[12] Universidad Tecnológica Nacional – Facultad Regional Buenos Aires, Buenos Aires, Argentina
[13] University of Adelaide, Adelaide, S.A., Australia
[14] Université Libre de Bruxelles (ULB), Brussels, Belgium
[15] Vrije Universiteit Brussels, Brussels, Belgium
[16] Centro Federal de Educação Tecnológica Celso Suckow da Fonseca, Petropolis, Brazil
[17] Instituto Federal de Educação, Ciência e Tecnologia do Rio de Janeiro (IFRJ), Brazil
[18] Universidade de São Paulo, Escola de Engenharia de Lorena, Lorena, SP, Brazil
[19] Universidade de São Paulo, Instituto de Física de São Carlos, São Carlos, SP, Brazil
[20] Universidade de São Paulo, Instituto de Física, São Paulo, SP, Brazil
[21] Universidade Estadual de Campinas, IFGW, Campinas, SP, Brazil
[22] Universidade Estadual de Feira de Santana, Feira de Santana, Brazil
[23] Universidade Federal de Campina Grande, Centro de Ciencias e Tecnologia, Campina Grande, Brazil
[24] Universidade Federal do ABC, Santo André, SP, Brazil
[25] Universidade Federal do Paraná, Setor Palotina, Palotina, Brazil
[26] Universidade Federal do Rio de Janeiro, Instituto de Física, Rio de Janeiro, RJ, Brazil
[27] Universidade Federal do Rio de Janeiro (UFRJ), Observatório do Valongo, Rio de Janeiro, RJ, Brazil
[28] Universidade Federal Fluminense, EEIMVR, Volta Redonda, RJ, Brazil
[29] Universidad de Medellín, Medellín, Colombia
[30] Universidad Industrial de Santander, Bucaramanga, Colombia

[31] Charles University, Faculty of Mathematics and Physics, Institute of Particle and Nuclear Physics, Prague, Czech Republic
[32] Institute of Physics of the Czech Academy of Sciences, Prague, Czech Republic
[33] Palacky University, Olomouc, Czech Republic
[34] CNRS/IN2P3, IJCLab, Université Paris-Saclay, Orsay, France
[35] Laboratoire de Physique Nucléaire et de Hautes Energies (LPNHE), Sorbonne Université, Université de Paris, CNRS-IN2P3, Paris, France
[36] Univ. Grenoble Alpes, CNRS, Grenoble Institute of Engineering Univ. Grenoble Alpes, LPSC-IN2P3, 38000 Grenoble, France
[37] Université Paris-Saclay, CNRS/IN2P3, IJCLab, Orsay, France
[38] Bergische Universität Wuppertal, Department of Physics, Wuppertal, Germany
[39] Karlsruhe Institute of Technology (KIT), Institute for Experimental Particle Physics, Karlsruhe, Germany
[40] Karlsruhe Institute of Technology (KIT), Institut für Prozessdatenverarbeitung und Elektronik, Karlsruhe, Germany
[41] Karlsruhe Institute of Technology (KIT), Institute for Astroparticle Physics, Karlsruhe, Germany
[42] RWTH Aachen University, III. Physikalisches Institut A, Aachen, Germany
[43] Universität Hamburg, II. Institut für Theoretische Physik, Hamburg, Germany
[44] Universität Siegen, Department Physik – Experimentelle Teilchenphysik, Siegen, Germany
[45] Gran Sasso Science Institute, L'Aquila, Italy
[46] INFN Laboratori Nazionali del Gran Sasso, Assergi (L'Aquila), Italy
[47] INFN, Sezione di Catania, Catania, Italy
[48] INFN, Sezione di Lecce, Lecce, Italy
[49] INFN, Sezione di Milano, Milano, Italy
[50] INFN, Sezione di Napoli, Napoli, Italy
[51] INFN, Sezione di Roma "Tor Vergata", Roma, Italy
[52] INFN, Sezione di Torino, Torino, Italy
[53] Istituto di Astrofisica Spaziale e Fisica Cosmica di Palermo (INAF), Palermo, Italy
[54] Osservatorio Astrofisico di Torino (INAF), Torino, Italy
[55] Politecnico di Milano, Dipartimento di Scienze e Tecnologie Aerospaziali , Milano, Italy
[56] Università del Salento, Dipartimento di Matematica e Fisica "E. De Giorgi", Lecce, Italy
[57] Università dell'Aquila, Dipartimento di Scienze Fisiche e Chimiche, L'Aquila, Italy
[58] Università di Catania, Dipartimento di Fisica e Astronomia "Ettore Majorana", Catania, Italy
[59] Università di Milano, Dipartimento di Fisica, Milano, Italy
[60] Università di Napoli "Federico II", Dipartimento di Fisica "Ettore Pancini", Napoli, Italy
[61] Università di Palermo, Dipartimento di Fisica e Chimica "E. Segrè", Palermo, Italy
[62] Università di Roma "Tor Vergata", Dipartimento di Fisica, Roma, Italy
[63] Università Torino, Dipartimento di Fisica, Torino, Italy
[64] Benemérita Universidad Autónoma de Puebla, Puebla, México
[65] Unidad Profesional Interdisciplinaria en Ingeniería y Tecnologías Avanzadas del Instituto Politécnico Nacional (UPIITA-IPN), México, D.F., México
[66] Universidad Autónoma de Chiapas, Tuxtla Gutiérrez, Chiapas, México
[67] Universidad Michoacana de San Nicolás de Hidalgo, Morelia, Michoacán, México
[68] Universidad Nacional Autónoma de México, México, D.F., México
[69] Universidad Nacional de San Agustin de Arequipa, Facultad de Ciencias Naturales y Formales, Arequipa, Peru
[70] Institute of Nuclear Physics PAN, Krakow, Poland
[71] University of Łódź, Faculty of High-Energy Astrophysics,Łódź, Poland
[72] Laboratório de Instrumentação e Física Experimental de Partículas – LIP and Instituto Superior Técnico – IST, Universidade de Lisboa – UL, Lisboa, Portugal
[73] "Horia Hulubei" National Institute for Physics and Nuclear Engineering, Bucharest-Magurele, Romania
[74] Institute of Space Science, Bucharest-Magurele, Romania
[75] University Politehnica of Bucharest, Bucharest, Romania
[76] Center for Astrophysics and Cosmology (CAC), University of Nova Gorica, Nova Gorica, Slovenia
[77] Experimental Particle Physics Department, J. Stefan Institute, Ljubljana, Slovenia

[78] Universidad de Granada and C.A.F.P.E., Granada, Spain
[79] Instituto Galego de Física de Altas Enerxías (IGFAE), Universidade de Santiago de Compostela, Santiago de Compostela, Spain
[80] IMAPP, Radboud University Nijmegen, Nijmegen, The Netherlands
[81] Nationaal Instituut voor Kernfysica en Hoge Energie Fysica (NIKHEF), Science Park, Amsterdam, The Netherlands
[82] Stichting Astronomisch Onderzoek in Nederland (ASTRON), Dwingeloo, The Netherlands
[83] Universiteit van Amsterdam, Faculty of Science, Amsterdam, The Netherlands
[84] Case Western Reserve University, Cleveland, OH, USA
[85] Colorado School of Mines, Golden, CO, USA
[86] Department of Physics and Astronomy, Lehman College, City University of New York, Bronx, NY, USA
[87] Michigan Technological University, Houghton, MI, USA
[88] New York University, New York, NY, USA
[89] University of Chicago, Enrico Fermi Institute, Chicago, IL, USA
[90] University of Delaware, Department of Physics and Astronomy, Bartol Research Institute, Newark, DE, USA
[91] University of Wisconsin-Madison, Department of Physics and WIPAC, Madison, WI, USA

—

[a] Louisiana State University, Baton Rouge, LA, USA
[b] also at University of Bucharest, Physics Department, Bucharest, Romania
[c] School of Physics and Astronomy, University of Leeds, Leeds, United Kingdom
[d] now at Agenzia Spaziale Italiana (ASI). Via del Politecnico 00133, Roma, Italy
[e] Fermi National Accelerator Laboratory, Fermilab, Batavia, IL, USA
[f] now at Graduate School of Science, Osaka Metropolitan University, Osaka, Japan
[g] now at ECAP, Erlangen, Germany
[h] Max-Planck-Institut für Radioastronomie, Bonn, Germany
[i] also at Kapteyn Institute, University of Groningen, Groningen, The Netherlands
[j] Colorado State University, Fort Collins, CO, USA
[k] Pennsylvania State University, University Park, PA, USA

Acknowledgments

The successful installation, commissioning, and operation of the Pierre Auger Observatory would not have been possible without the strong commitment and effort from the technical and administrative staff in Malargüe. We are very grateful to the following agencies and organizations for financial support:

Argentina – Comisión Nacional de Energía Atómica; Agencia Nacional de Promoción Científica y Tecnológica (ANPCyT); Consejo Nacional de Investigaciones Científicas y Técnicas (CONICET); Gobierno de la Provincia de Mendoza; Municipalidad de Malargüe; NDM Holdings and Valle Las Leñas; in gratitude for their continuing cooperation over land access; Australia – the Australian Research Council; Belgium – Fonds de la Recherche Scientifique (FNRS); Research Foundation Flanders (FWO); Brazil – Conselho Nacional de Desenvolvimento Científico e Tecnológico (CNPq); Financiadora de Estudos e Projetos (FINEP); Fundação de Amparo à Pesquisa do Estado de Rio de Janeiro (FAPERJ); São Paulo Research Foundation (FAPESP) Grants No. 2019/10151-2, No. 2010/07359-6 and No. 1999/05404-3; Ministério da Ciência, Tecnologia, Inovações e Comunicações (MCTIC); Czech Republic – Grant No. MSMT CR LTT18004, LM2015038, LM2018102, CZ.02.1.01/0.0/0.0/16_013/0001402, CZ.02.1.01/0.0/0.0/18_046/0016010 and CZ.02.1.01/0.0/0.0/17_049/0008422; France – Centre de Calcul IN2P3/CNRS; Centre National de la Recherche Scientifique (CNRS); Conseil Régional Ile-de-France; Département Physique Nucléaire et Corpusculaire (PNC-IN2P3/CNRS); Département Sciences de l'Univers (SDU-INSU/CNRS); Institut Lagrange de Paris (ILP) Grant No. LABEX ANR-10-LABX-63 within the Investissements d'Avenir Programme Grant No. ANR-11-IDEX-0004-02; Germany – Bundesministerium für Bildung und Forschung (BMBF); Deutsche Forschungsgemeinschaft (DFG); Finanzministerium Baden-Württemberg; Helmholtz Alliance for Astroparticle Physics (HAP); Helmholtz-Gemeinschaft Deutscher Forschungszentren (HGF); Ministerium für Kultur und Wissenschaft des Landes Nordrhein-Westfalen; Ministerium für Wissenschaft, Forschung und Kunst des Landes Baden-Württemberg; Italy – Istituto Nazionale di Fisica Nucleare (INFN); Istituto nazionale di Astrofisica (INAF); Ministero dell'Universitá e della Ricerca (MUR); CETEMPS Center of Excellence; Ministero degli Affari Esteri (MAE), ICSC Centro Nazionale di Ricerca in High Performance Computing, Big Data and Quantum Computing, funded by European Union NextGenerationEU, reference code CN_00000013; México – Consejo Nacional de Ciencia y Tecnología (CONACYT) No. 167733; Universidad Nacional Autónoma de México (UNAM); PAPIIT DGAPA-UNAM; The Netherlands – Ministry of Education, Culture and Science; Netherlands Organisation for Scientific Research (NWO); Dutch national e-infrastructure with the support of SURF Cooperative; Poland – Ministry of Education and Science, grants No. DIR/WK/2018/11 and 2022/WK/12; National Science Centre, grants No. 2016/22/M/ST9/00198, 2016/23/B/ST9/01635, 2020/39/B/ST9/01398, and 2022/45/B/ST9/02163; Portugal – Portuguese national funds and FEDER funds within Programa Operacional Factores de Competitividade through Fundação para a Ciência e a Tecnologia (COMPETE); Romania – Ministry of Research, Innovation and Digitization, CNCS-UEFISCDI, contract no. 30N/2023 under Romanian National Core Program LAPLAS VII, grant no. PN 23 21 01 02 and project number PN-III-P1-1.1-TE-2021-0924/TE57/2022, within PNCDI III; Slovenia – Slovenian Research Agency, grants P1-0031, P1-0385, I0-0033, N1-0111; Spain – Ministerio de Economía, Industria y Competitividad (FPA2017-85114-P and PID2019-104676GB-C32), Xunta de Galicia (ED431C 2017/07), Junta de Andalucía (SOMM17/6104/UGR, P18-FR-4314) Feder Funds, RENATA Red Nacional Temática de Astropartículas (FPA2015-68783-REDT) and María de Maeztu Unit of Excellence (MDM-2016-0692); USA – Department of Energy, Contracts No. DE-AC02-07CH11359, No. DE-FR02-04ER41300, No. DE-FG02-99ER41107 and No. DE-SC0011689; National Science Foundation, Grant No. 0450696; The Grainger Foundation; Marie Curie-IRSES/EPLANET; European Particle Physics Latin American Network; and UNESCO.